PROCEEDINGS OF SPIE

SPIEDigitalLibrary.org/conference-proceedings-of-spie

Optimizing EUV imaging metrics as a function of absorber thickness and illumination source: simulation case study of Ta-Co alloy

Devesh Thakare, Annelies Delabie, Vicky Philipsen

Devesh Thakare, Annelies Delabie, Vicky Philipsen, "Optimizing EUV imaging metrics as a function of absorber thickness and illumination source: simulation case study of Ta-Co alloy," Proc. SPIE 12472, 37th European Mask and Lithography Conference, 124720A (1 November 2022); doi: 10.1117/12.2640098

SPIE.

Event: 37th European Mask and Lithography Conference, 2022, Leuven, Belgium

Optimizing EUV Imaging Metrics as a Function of Absorber Thickness and Illumination Source: Simulation Case Study of Ta-Co alloys

Devesh Thakare[a,b], Annelies Delabie[a,b], Vicky Philipsen*[a]

[a]imec, Kapeldreef 75, B-3001 Leuven, Belgium;
[b]KU Leuven, Department of Chemistry, Leuven, Belgium;

Abstract: The imaging performance of a mask in EUV lithography is governed by the optical properties of the absorber material, namely the refractive index *n* and extinction coefficient *k*, and by its thickness. The imaging metrics viz. Normalized Intensity Log Slope (NILS), Telecentricity Error (TCE) and Best Focus Variation (BFV) through pitch, exhibit a tradeoff. In addition, the choice of illumination has a significant influence on these imaging metrics. Most of the previous studies have focused on either reflectivity or phase shift induced by the absorber to determine the optimum absorber thickness. The limitation of this approach is that the structure of the patterns on the mask is ignored. This simulation study is intended to facilitate the selection of the optimum absorber thickness with an emphasis on diffraction order analysis and the impact of illumination source shape using a case study of TaCo alloy. The behavior of imaging metrics is investigated as a function of absorber thickness in combination with illumination source shapes recommended in the literature. Maximal NILS, TCE within specified limits, balancing of diffraction order amplitudes with a minimum phase difference, and throughput criterion, are the important parameters that are considered when selecting the optimum absorber thickness. We evaluate and compare the through pitch imaging performance of TaCo alloy with recommended thicknesses, to that of the reference TaBN 60 nm absorber using Leaf shape Dipole (LDP), Inner Half Leaf shape Dipole (IHLDP) and Outer Half Leaf shape Dipole (OHLDP) for Line and Space (LnS) pattern with trench width of 10nm and the smallest pitch of 20 nm. The study confirms that TaCo alloy exhibits improved NILS and lower BFV compared to the reference TaBN 60 nm absorber.

Keywords: EUV lithography, EUV mask absorbers, High-k mask absorbers, High-NA, Photomasks.

1. Introduction

When simulation studies demonstrated the significant impact of mask absorbers on image quality at the wafer level for EUV imaging, a resurgence of interest in studies related to materials for EUV mask absorbers is observed in recent times [1]. The imaging performance of a mask in EUV lithography is governed by the optical properties of the absorber material, namely the refractive index n and extinction coefficient k, and by its thickness. Absorber materials are characterized as high absorption, attenuated phase shifting, or vacuum phase matching depending on their optical properties relative to the reference TaBN absorber. The imaging metrics viz. Normalized Intensity Log Slope (NILS), Telecentricity Error (TCE) and Best Focus Variation (BFV) through pitch, exhibit a tradeoff as a function of absorber material and thickness. Therefore, determining the right combination of absorber material and thickness that optimizes these imaging metrics becomes absolutely essential. Most of the previous studies have focused on either reflectivity or phase shift induced by the absorber to determine the optimum absorber thickness. The limitation of this approach is that the structure of the patterns on the mask is ignored. Studies focusing on the mask diffraction analysis have enhanced our understanding about imaging effects [2],[3],[4]. Findings of these studies indicate that diffraction order analyses should not be neglected to determine the optimum absorber thickness. Moreover, studies have reported that the absorber material choice also affects the optimum source shape [5]. According to Erdmann A. et. al, the outcome of an absorber material and thickness optimization study will be strongly influenced by the lithography metrics and specific use cases [5]. Furthermore, lithographers are well aware of the impact of mask bias, wafer focus and illumination source shape on the imaging metrics. Erdmann A. et. al recommend considering multiple objectives such as NILS, depth of focus, TCE and source filling in the mask stack optimization [5]. With several variables to consider, determining the right absorber thickness becomes challenging. In this paper, we therefore propose a step-by-step methodology to simplify the process and guide the simulation flow.

37th European Mask and Lithography Conference, edited by Uwe Behringer,
Proc. of SPIE Vol. 12472, 124720A · © 2022 SPIE
0277-786X · doi: 10.1117/12.2640098

In a previous study, we investigated Ta-Co alloys as prospective high-k mask absorbers using both experimental and theoretical methods. We compared the film morphology, surface composition and chemical stability by means of experiments and discussed the imaging performance through aerial image simulations [6]. This simulation study is intended to facilitate the selection of the optimum absorber thickness with an emphasis on diffraction order analysis and the impact of illumination source shape using a case study of TaCo alloy. The behavior of imaging metrics is investigated as a function of absorber thickness in combination with illumination source shapes recommended in literature. Maximal NILS, TCE within specified limits, balancing of diffraction order amplitudes with a minimum diffraction phase difference, and maximal throughput, are the important parameters that are considered when selecting the optimum absorber thickness. Our simulations aimed at Line and Space (LnS) patterns with a target CD (Critical Dimension) of 10 nm in a pitch of 20 nm (10nmP20) for High-NA (Numerical Aperture) 0.55 EUV lithography that matches the industry goal by 2028 [7].

2. Methodology

2.1 Simulation Setup

This study uses S-Litho EUV software by Synopsys® to simulate the imaging performance. The mask topography and the optical properties of the mask materials are taken into consideration by S-Litho EUV while performing rigorous EMF (Electro Magnetic Field) simulations. A 20% central obscuration in an anamorphic projection mirror and CRAO (Chief Ray Angle at Object) of 5.355^{o} for EUV light source having a wavelength of 13.5 nm are the typical scanner inputs for simulations [7]. Our simulations make use of the Mo/Si Multi-Layer (ML) mirror mask model described by Makhotkin et al. [8]. The absorber stack is defined using the experimentally determined optical constants n and k of Ta-Co alloys [6].

2.1 Background for setting up simulation methodology

Next-generation EUV lithography utilizes reflective optics instead of transmissive optics for pattern transfer, in contrast to conventional lithography. A Bragg reflector with patterned absorber material on top, makes up a standard EUV mask. TaBN serves as the absorber material in current EUV masks. Figure 1 depicts a schematic representation of illumination on an EUV mask . A periodic structure of LnS pattern represented with absorber and reflective areas on a mask act as a diffraction grating. When a mask is illuminated, light gets diffracted due to absorber on it way reaching the ML mirror. The reflected light from the ML mirror encounters the absorber layer again and gets diffracted for the second time. Claire van Lare et al. [9] and A. Erdmann et al. [10] have discussed the double diffraction model in detail. For simplicity, only zeroth and first diffraction orders have been illustrated in Figure 1. This diffracted plus double diffracted light is captured by the NA of the imaging system and diverted through series of projection mirrors to reconstruct the original image at the wafer level. Due to the physical limitation of the optical components, not all of the diffraction orders can be captured by the imaging system. The image fidelity at the wafer level increases with the number of diffraction orders captured which is determined by the NA of the exposure tool. A minimum of two diffraction orders are required that can interfere to form an image.

Diffraction of light at the mask can be mathematically expressed as Fourier Transform (FT) of a mask (Mask Transform Function). The diffraction orders consist of several even and odd harmonics, frequency and amplitude of each harmonic can be calculated using FT theory. Since the absorber material is not ideal, it is neither fully transmissive nor absorptive in nature. Therefore, the amplitude and phase of the diffraction orders depends on the transmissivity of the absorber which in turn depends on the thickness of the absorber. The transmissivity decreases as the absorber thickness increases. Thus, the properties of diffraction orders vary as a function of absorber thickness which will be discussed in section 3 later.

Figure 1 also depicts a cross section of the mask model with optical properties per slice as seen by the simulation software that uses waveguide approach to solve Maxwell's electromagnetic equations. The electromagnetic field boundary conditions are properly formulated to couple the fields between adjacent slices. The system's response to how the output light is diffracted and reflected in relation to the incident planar wave is described by iterative coupling of all slices [11]. The final output of the simulation tool is the aerial image formed by combined interference of the diffraction orders collected by the projection optics

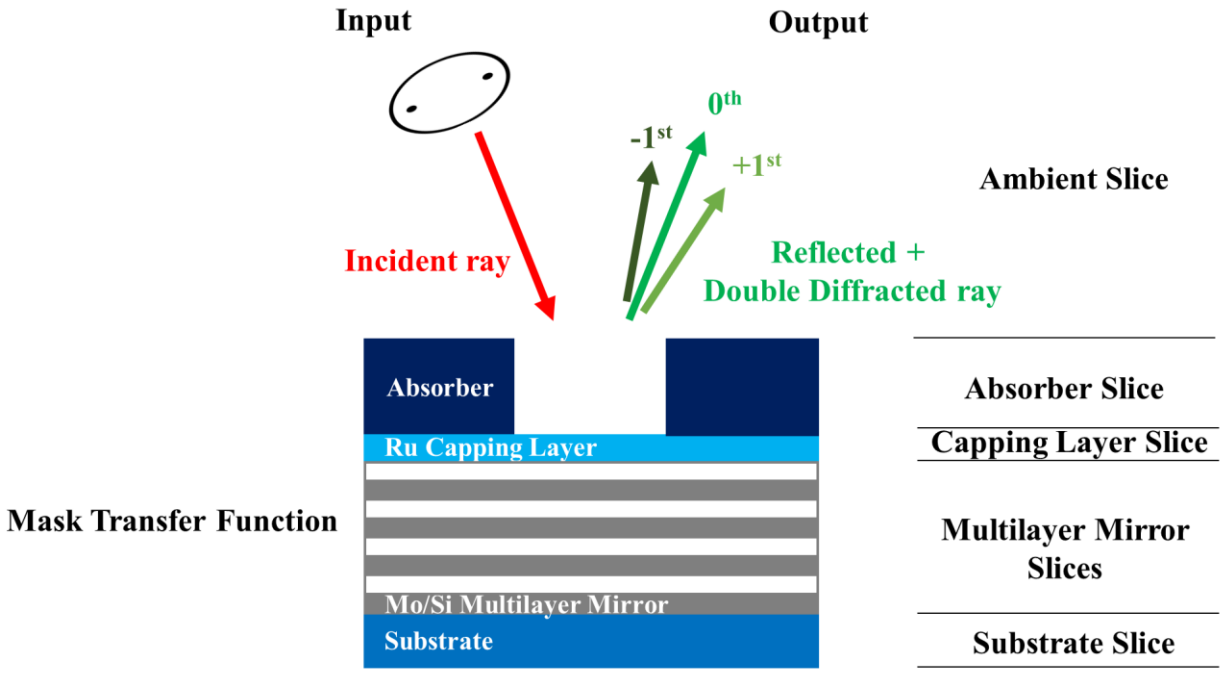

Figure 1. Simple schematic showing the illumination of an EUV mask with incident ray in red and diffracted plus double diffracted rays in shades of green. Additionally, it depicts the mask model sliced with consistent optical properties as seen by the simulation software that uses waveguide approach to solve the Maxwell's electromagnetic equations

In this simulation study, our first step is to optimize the absorber thickness. As previously stated, the mask topography and material (*n* & *k* and thickness), the mask feature width (mask bias), and illumination all impact NILS. This leads to a multivariable optimization that further increases the complexity. A Telecentric Sigma Point Source (TS-PS) is employed as an illumination source to simplify the steps involved in the absorber thickness optimization process. As a function of focus, NILS remains constant for a TS-PS [12] which eliminates the necessity of an additional variable (focus). This saves a significant number of computations, resulting in a shorter simulation cycle time. The TS-PS illumination chosen for this simulation study corresponds to the smallest pitch that needs to be printed at the wafer level. This can be calculated for equal line and space patterns as given in Eq. 1 and for Contact Holes (CH) in a square array as given in Eq. 2.

$$Telecentric\ \sigma\ for\ LnS = \frac{\lambda}{2\ NA\ P} \qquad Equation\ 1$$

$$Telecentric\ \sigma\ for\ CH = \frac{\lambda}{\sqrt{2}\ NA\ P} \qquad Equation\ 2$$

where σ indicates the position of point source in the pupil plane, λ denotes the wavelength of the illumination, NA is the numerical aperture, and P is the pattern pitch.

According to fundamentals of optics, when all of the diffracted beams arrive at the image plane with symmetrical incidence angles and are in-phase in any plane perpendicular to the path of propagation, an unlimited depth of focus can be attained. The necessary conditions for this phenomenon to occur are met when the requirements mentioned in Equations 1 and 2 are satisfied.

The threshold-to-size (TtS) is the level of aerial image intensity at which the target CD of a feature is determined. The TtS is inversely proportional to the required exposure dose. An additional metric known as Throughput Criterion (TpT) (Eq. 3) was taken into account to address this tradeoff [13]. It is an indicator that considers a good balance between NILS and TtS. TpT is used for narrowing down the absorber thickness range while determining the optimum absorber thickness.

$$Throughput\ Criterion\ (TpT) = NILS\sqrt{TtS} \qquad Equation\ 3$$

The NILS depends on the phase and amplitude of the diffracted orders as expressed in Equation 4 [3]. The NILS is maximized when the diffraction order amplitude ratio and the cosine of the phase difference are close to 1.

$$NILS \propto \frac{2\,A_1/A_0}{1+(A_1/A_0)^2}\cos\phi \qquad Equation\ 4$$

where A_1 and A_0 are the amplitudes of 1st and 0th diffraction orders respectively and ϕ is the phase difference between them

As stated earlier, the properties of diffraction orders depend on the thickness of the absorber in addition to other factors such as ML mirror and angle of incidence. Therefore, the thickness of the absorber affects NILS as well.

2.3 Absorber thickness optimization methodology

The proposed absorber thickness optimization methodology is depicted in Figure 2 and is based on the literature review discussed in the previous sub-section. In the first step, select the TS-PS illumination for the smallest targeted pitch. A TS-PS dipole for LnS pattern and TS-PS quasar for CH pattern are recommended. For LnS pattern, simulations for both horizontal and vertical orientation are suggested; a proper evaluation of results obtained from both orientations of simulations have proven beneficial in order to draw the final conclusion about the absorber thickness.

In the second step, absorber thickness and mask bias (trench width) is varied simultaneously. The trench width on the mask is varied in small steps (around target CD). For each combination of the absorber thickness and the mask bias, the TtS value that prints the target CD is calculated, and the corresponding NILS is reported.

In step three, the data generated from the previous step is utilized to find the combination of mask bias and absorber thickness that results in the maximum NILS. In step four, for each incremental step of absorber thickness, extraction of TtS, mask bias, diffraction order amplitude ratio and phase relation corresponding to the maximum NILS obtained in step three is done. Then these values are plotted as a function of absorber thickness.

In the last, fifth step, the optimum absorber thickness is proposed by analyzing all the plots obtained in the previous step. We deliberately seek absorber thickness having diffraction order amplitude ratio close to 1 with minimum phase difference and optimum TpT. In addition, a local peak in the NILS plot is preferred to minimize the sensitivity towards absorber thickness variations.

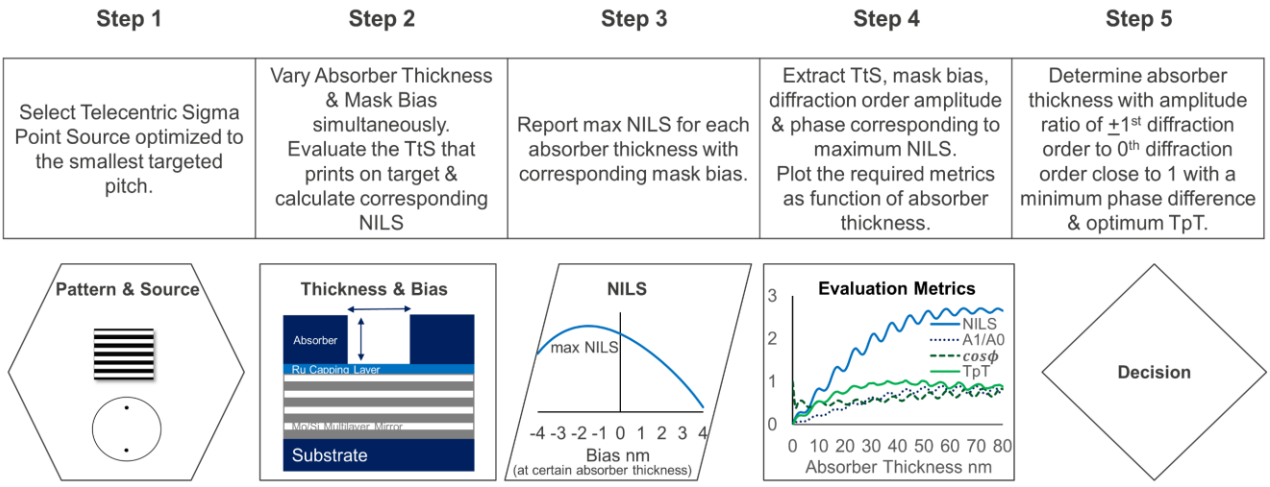

Figure 2. Optimization flow of absorber thickness depicted with help of a simplified flow chart.

2.4 Setting simulation goals and defining target values

Next, we explain the target values for imaging metrics and their significance. For an effective pattern transfer, a NILS value larger than 2 is regarded as acceptable [14]. A higher NILS implies lower defectivity [15] and a lower sensitivity to intensity threshold variations. TCE (also known as pattern shift through focus) signifies the lateral pattern shift of a feature as a function of focus and is represented in mrad or nm/um. When the CRAO is not perfectly parallel to the feature orientation, this causes an imbalance in the +1 and -1 diffraction order intensities, resulting in mask induced pattern shift through focus [16]. This results in pattern-dependent Edge Placement Errors (EPE).

The overall focus budget for high NA EUV lithography is estimated to be 35 nm [17]. A 10 mrad TCE implies 1 nm pattern shift per 100 nm of defocus. Eelco van Setten et al. [16] suggest that the M3D induced TCE should be kept under 20 mrad. TCE and focus budget can be used to compute the M3D-induced overlay error using Equation 5 [16]. The targeted overlay control for a high-NA application is 1.1 nm or below [18]. The M3D-induced overlay error accounts to be 0.175 nm for a focus budget of 35 nm and TCE of 10 mrad (10 mrad x 0.035µm/2), thus consuming ~16% of the overlay budget. TCE restricted to 10 mrad, shouldn't have a significant impact on the overlay budget as per the opinion of Eelco van Setten et al. [13]. As a result, we aim to target a TCE of 10 mrad or below for the smallest pitch.

$$M3D\ induced\ overlay\ =\ TCE\ x\ Focus\ Budget\ half\ range \qquad Equation\ 5$$

To assess the focus behavior through pitch at fixed absorber thickness, we varied the LnS pitch from 20 nm to 40 nm with a 4 nm increment, all targeting the same CD. The best focus for a particular pitch is the focus value that produces the highest NILS. The best focus variation through pitch (BFV) is defined as the difference between the maximum and minimum value of the best focus across the pitches. In order to print the different pitches with the largest possible overlapping process window, the BFV should be as small as possible.

The choice of illumination source has a substantial impact on the evaluation metrics NILS, TCE, BFV and TtS. To increase NILS for Ta-based absorbers, Franke et al. [12] recommend using either an inner half leaf or an outer half leaf shape dipole to avoid NILS loss arising from fading. Fading occurs when the aerial images that are shifted against one another are superimposed [12]. We intend to verify whether this phenomenon is also true for TaCo alloy. Therefore, we employed three illumination sources in our simulation study, viz. Leaf shape Dipole (LDP), Inner Half Leaf shape Dipole (IHLDP) and Outer Half Leaf shape Dipole (OHLDP) (Figure 3). The illumination sources are optimized for the smallest pitch.

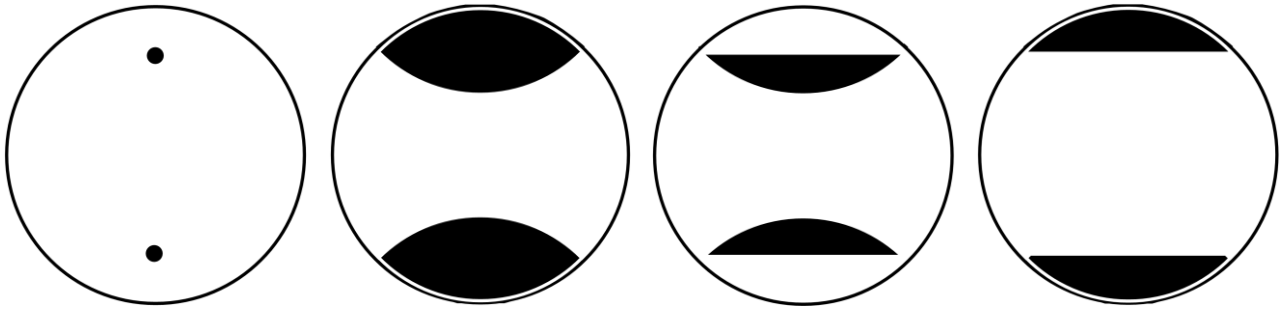

Figure 3. Illumination source shapes for horizontal LnS patterns (a) TS-PS, (b) LDP, (c) IHLDP, and (d) OHLDP

3. Results and Discussions

Following is a brief overview of sections involved in our simulation study. Firstly, we validate our absorber thickness optimization methodology with the reference TaBN absorber. Secondly, we propose an optimized absorber thickness for TaCo alloy using our step-by-step methodology simulation guide. Thirdly, we compare the imaging metrics for the TaCo alloy absorber using LDP, IHLDP and OHLDP illumination sources through thickness for the smallest pitch. Finally, we compare the through pitch performance of different illumination source shapes for reference TaBN absorber and the selected thickness of TaCo alloy absorber.

3.1 Validation of absorber thickness optimization methodology with reference TaBN absorber

First, we simulate NILS for horizontal (Hor) and vertical (Ver) lines and space patterns at a single pitch of 20 nm for the TaBN absorber by varying absorber thickness and mask bias using the telecentric sigma point source (Figure 4). The diffraction order amplitude ratio and the diffraction order phase are obtained at the telecentric sigma point. The orientation of LnS is either horizontal, i.e., orthogonal to the CRAO on the mask or vertical, i.e., parallel. Due to oblique illumination of the mask, asymmetry is observed in the diffraction pattern [19]. The well-known shadowing effect for horizontal features results from the height of the mask absorber (thickness) blocking part of the incident and reflected light from the ML mirror. The shadowing effect is prominently observed for the pole that is placed at larger incidence angle. Thus, the imaging metrics strongly depend on the orientation of the pattern with respect to the illumination. Therefore, horizontal LnS pattern is given a preference during the optimal absorber selection process.

The reference absorber thickness is 60 nm, and this indeed corresponds to a local maximum in the swing curve of NILS plot (Figure 4 (a)). At this absorber thickness, the amplitude ratio of the -1 diffraction order and the zeroth diffraction order for a horizontal LnS pattern is close to 1 (Figure 4 (b)). The cosine of the phase difference for -1 diffraction order indicates a rising trend with increasing absorber thickness but not able to reach close to 1. This behavior mainly depends on the optical properties of the absorber material; in addition, shape of the absorber (side wall angle) and mask bias also plays an important role.

The amplitude ratio of the +1 diffraction order and zeroth diffraction order starts to saturate around 60 nm (solid blue line in Figure 4 (b)). The cosine of the phase difference for +1 diffraction order exhibits a declining trend in the swing behavior beyond absorber thickness of 65 nm (Figure 4 (c)). A possible explanation for these observations is the shadowing effect on horizontal LnS, where the +1 diffraction order is being blocked by a thicker absorber.

Figure 4 (d) shows the throughput criterion as a function of absorber thickness. In the absorber thickness range of around 52 nm to 65 nm, a saturation in the swing behavior is observed. Thus the 60 nm thickness of reference TaBN absorber can be justified by our absorber thickness optimization methodology.

A similar analysis could be done for vertical LnS patterns for which +1 and -1 diffraction orders are identical since they are not affected by the shadowing effect observed in EUV lithography.

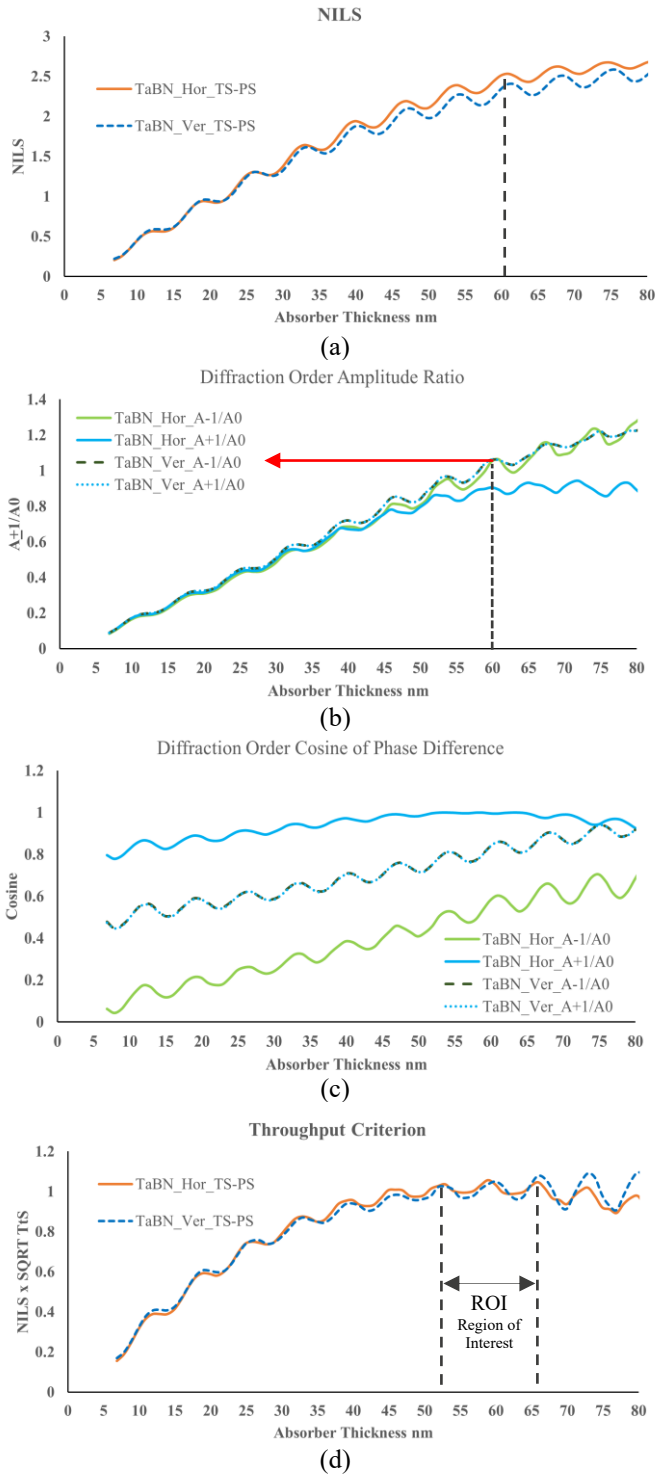

Figure 4. Simulation comparison of horizontal and vertical line and space pattern for 10nmP20. Imaging metrics plotted as a function of absorber thickness for TaBN with TS-PS (a) NILS, (b) diffraction orders amplitude ratio (c) diffraction orders cosine phase and (d) throughput criterion. all values obtained at telecentric sigma

3.2 Optimizing absorber thickness for TaCo alloy

A similar procedure is followed to obtain the optimum absorber thickness of TaCo alloy. We perform a through-thickness evaluation for the TaCo alloy absorber. We start by optimizing the imaging metrics for horizontal (Hor) and vertical (Ver) lines and space patterns at a single pitch of 20 nm for the TaCo alloy absorber (Figure 5). For horizontal LnS patterns, the peak in the NILS plot tends to saturate for absorber thicknesses of 50 nm and above. Interestingly, at the point of NILS saturation, the amplitude ratio of the -1 diffraction order versus the zeroth diffraction order (A_{-1}/A_0) is close to 1 (Figure 5 (b)). Beyond 50 nm of absorber thickness, the imbalance in the diffraction order amplitudes of -1 and zeroth order is observed as growing oscillation that swings around ratio value of 1. Also, the amplitude ratio of the +1 diffraction order and zeroth diffraction order for the horizontal LnS pattern reaches a plateau region in the swing pattern at 50 nm and then gradually decreases with increasing absorber thickness.

Figure 5 (c) presents the cosine of the phase difference for +1 and -1 diffraction orders with respect to the zeroth order phase of the horizontal LnS pattern pitch 20 nm (indicated with solid lines). The cosine of the phase difference for -1 diffraction order indicates a rising trend with increasing absorber thickness but not able to reach close to 1 which is similar to the reference TaBN absorber. The cosine of the phase difference for +1 diffraction order shows a downward trend for absorber thickness greater than 55 nm.

Therefore, after considering the saturation of amplitude ratio and trends observed in cosine plots, we can conclude that, increasing absorber thickness beyond 55nm does not show significant improvement in NILS. Another phenomenon worth noticing is that the amplitude ratio's as well as the cosine phase's peak and valley points, of corresponding diffraction orders, do not corresponds to the same thickness value (slight offset). Therefore, both factors require careful consideration while observing the trend in the NILS plot. Due to TaCo alloy's lower *n* value than TaBN, the swing in the behavior of all the TaCo alloy curves is stronger than that of the reference TaBN absorber (light propagates faster in an optically rare medium).

Though NILS shows a gradual upward trend for absorber thicknesses above 55 nm, the throughput criterion indicates a modest downward trend for horizontal LnS pattern (Figure 5 (d)), due to decreasing TtS with increasing absorption. Therefore, the recommended Region of Interest (ROI) comprises between the two peaks as highlighted in Figure 5. Based on all aspects, we recommend an absorber thickness of 52 nm for the TaCo alloy.

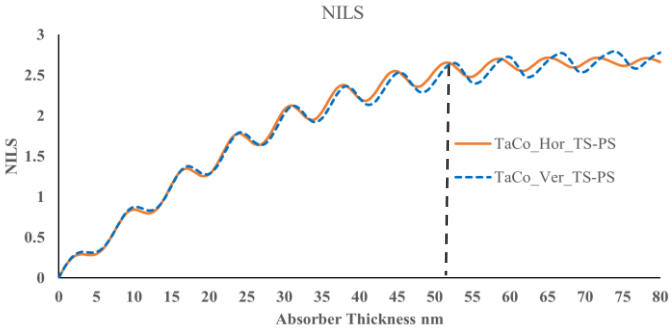

(a)

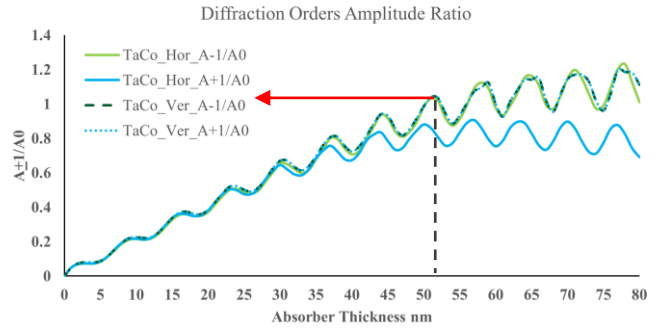

(b)

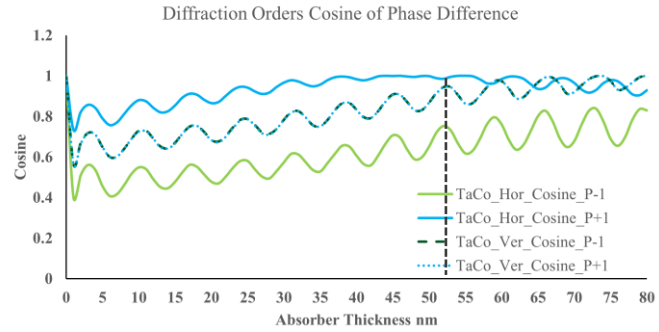

(c)

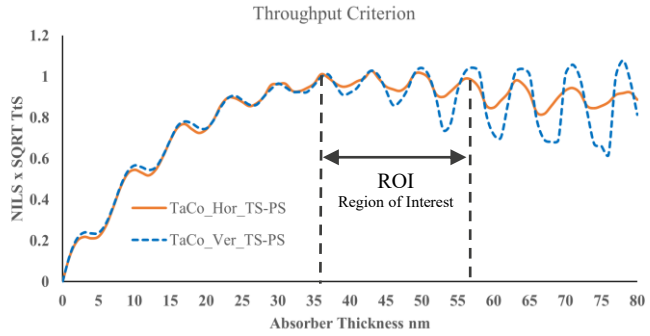

(d)

Figure 5. Simulation comparison of horizontal and vertical line and space pattern for 10nmP20. Imaging metrics plotted as a function of absorber thickness for TaCo alloy with TS-PS (a) NILS, (b) diffraction orders amplitude ratio (c) diffraction orders cosine phase and (d) throughput criterion. all values obtained at telecentric sigma.

3.3 Imaging metrics comparison of TaCo alloy absorber through thickness using different illumination sources

In this third section, we evaluate the imaging metrics for TaCo alloy absorber through thickness using LDP, IHLDP and OHLDP illumination sources for the smallest pitch of horizontal LnS pattern. As previously stated, illumination source shapes have a strong influence on the imaging metrics, we intend to study the behaviour of these imaging metrics through absorber thickness using different illuminations source shapes. Figure 6 (a) compares NILS obtained by different illumination source shapes to TS-PS illumination. We observe that using either IHLDP or OHLDP illumination source improves NILS in comparison to full LDP due to reduction in fading effect. As stated earlier, fading results from the superposition of two aerial images that are shifted with respect to one another [12]. These findings are consistent with Franke et al.'s [12] results, obtained for TaBN absorber. The NILS plot obtained using TS-PS closely resembles to that of LDP and follows the same swing pattern through thickness as the other illumination sources under investigation. Thus, we can conclude that TS-PS can be used as a true representative of the illumination source shapes to investigate NILS behaviour through thickness for the purpose of optimizing absorber thickness. Theoretically, a TS-PS illumination source will neither result in any form of telecentricity error nor its best focus position will vary. As a result, it is excluded from the comparison.

TCE values calculated for the three illumination source shapes are compared in Figure 6(b). TCE values reported in the plot correspond to the same mask bias used for the NILS plot. IHLDP has the least TCE, followed by LDP that exhibit moderate TCE. OHLDP demonstrates highest TCE in comparison to LDP and IHLDP. The reflectivity of an EUV ML is known to be sensitive to the angle of incidence of the illumination source. For OHLDP, the two half leaf shape poles are placed at the extreme incidence angles that causes imbalance of intensity in diffraction orders resulting in increased TCE. Similarly, for IHLDP, the two half poles are placed closer to the CRAO that results in less imbalance of diffraction order intensities and hence lower TCE. For LDP, TCE values can be considered as the average of both IHLDP and OHLDP resulting in moderate TCE. With increasing absorber thickness, the shadowing effect becomes prominent which contributes to the increasing deviation of the TCE.

Figure 6 (c) shows the best focus position of the aerial images for the three illumination sources as a function of absorber thickness. We observe the splitting of the best focus with opposite signs for IHLDP and OHLDP illumination source along the focus behaviour of LDP. When compared to TCE curves, the best focus curves of IHLDP and OHLDP flip their relative position along LDP. These results reflect the generic phenomenon arising due the presence of phase differences between two interfering diffraction orders as mentioned by Franke et al. [12]. The trade-off between the NILS and TCE is apparent from the graphs, implying that if NILS is given a precedence, TCE needs to be compromised. Observing the swing behaviour in the NILS plot with that of best focus plot, it is worth noticing that the NILS peaks correspond to the point where the difference between the best focus of IHLDP and OHLDP is small, and the NILS valley corresponds to the point where the difference between the best focus of IHLDP and OHLDP is large.

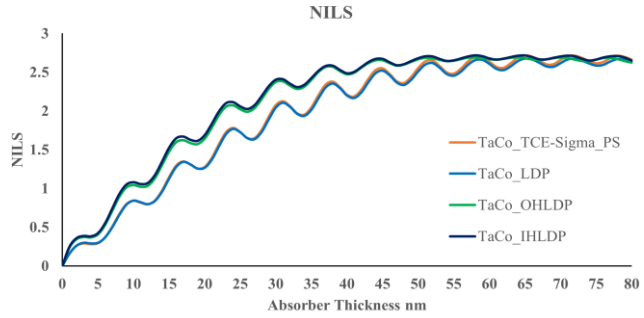

(a)

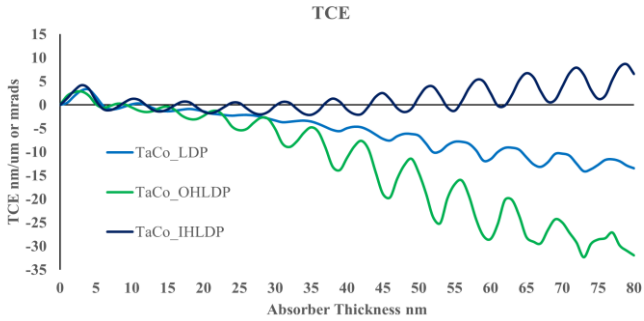

(b)

(c)

Figure 6. Comparison of imaging metrics of horizontal line and space pattern for 10nmP20. Imaging metrics plotted as a function of absorber thickness and various illumination source shapes for TaCo alloys with LDP, IHLDP and OHLDP (a) NILS, (b) TCE (c) Best Focus

3.4 Through-Pitch performance

In the final fourth section, we compare the through-pitch performance of horizontal and vertical LnS patterns using different illumination source shapes for the reference TaBN absorber with a thickness of 60 nm and the TaCo alloy absorber with a thickness of 52 nm. Figure 7 presents the through-pitch performance for the TaBN absorber with horizontal LnS pattern. IHLDP and OHLDP leads to an improvement in NILS for the smallest pitch in comparison to a LDP illumination source as predicted by Franke et al. [12]. However, this phenomenon is not consistent through pitch. We need to recall here the fact that the High-NA 0.55 lithography system employs a central obscuration. For the larger pitches, whose diffraction orders lie in the obscuration area, the NILS deteriorates because a part of diffraction orders are blocked. In addition, the number of diffraction orders captured also depends on the type of illumination source shape, the pitch and NA.

As observed in Figure 7 (b), the IHLDP illumination source exhibits the largest BFV, followed by the OHLDP and the LDP illumination source shows the smallest BFV. A slightly different trend is observed in TCE behavior of through pitch performance: the IHLDP illumination source demonstrates the smallest TCE followed by the LDP illumination source, while the OHLDP has the highest TCE. This phenomenon is a consequence arising from the placement of the poles relative to the CRAO in an illumination source, as previously stated. TtS does not differ significantly between the three illumination sources, see Figure 7 (d). As a result, the throughput criterion plot simply follows the NILS plot's trend (Figure 7 (e)). The mask bias used for each pitch to print on target is indicated in Figure 7 (f). The mask bias is calculated as (mask CD–target CD). The mask bias for each pitch is optimized to obtain highest NILS at the fixed TtS. Overall, trade-offs are observed between different imaging metrics as a function of illumination source shape.

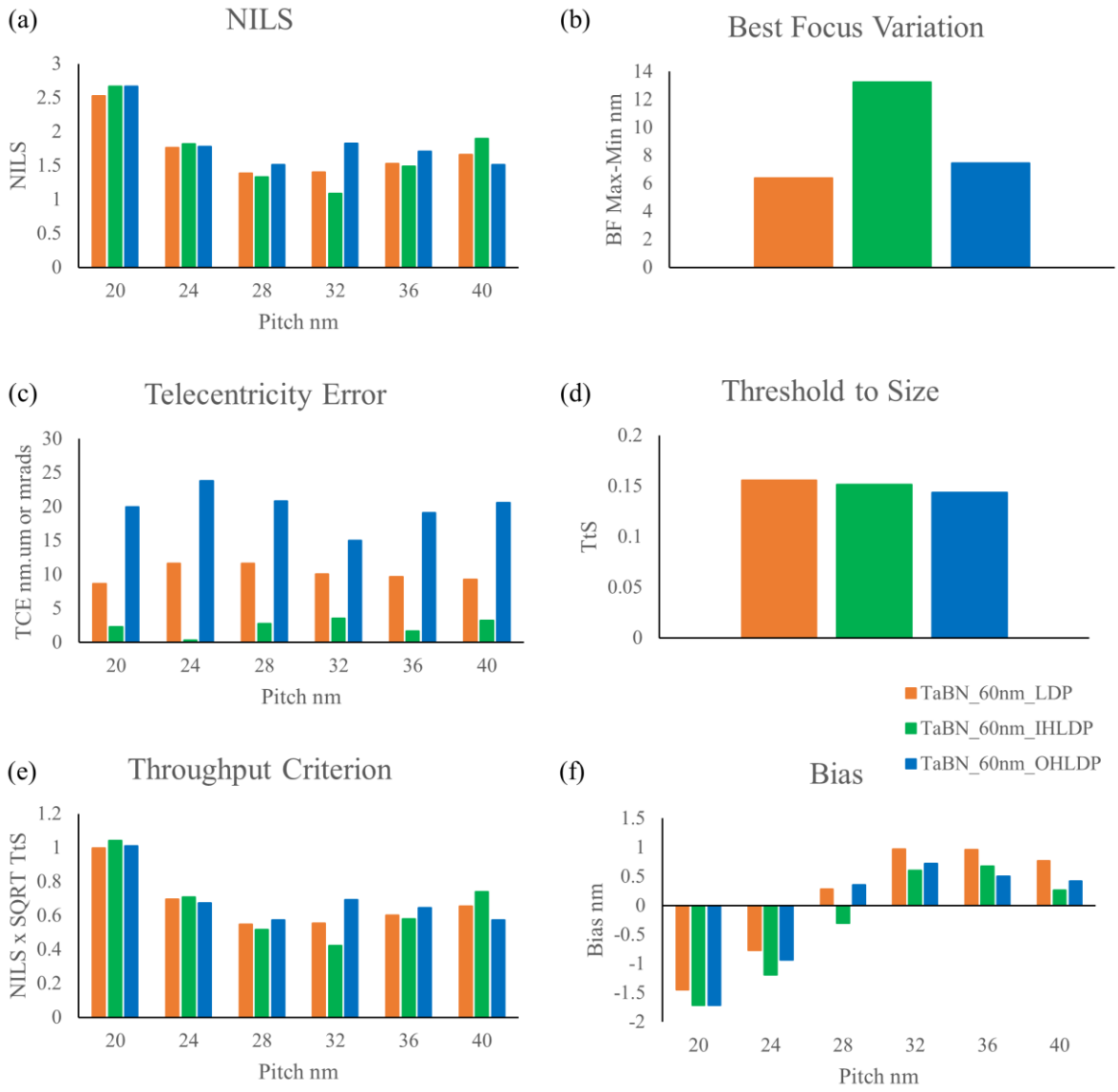

Figure 7. Comparison of the through-pitch imaging performance of reference TaBN absorber for horizontal LnS pattern using different illumination source shapes (a) NILS, (b) best focus variation through pitch, (c) telecentricity error, (d) threshold-to-size, (e) throughput criterion, (f) mask bias.

A similar through-pitch comparison of different imaging metrics is done for the TaCo alloy absorber with horizontal LnS pattern using different illumination source shapes (Figure 8). We observe a similar pattern in the NILS plot (Figure 8 (a)) when compared to the NILS plot of the reference TaBN absorber (Figure 7 (a)). However, due to its higher extinction coefficient k, the TaCo alloy absorber demonstrates improved NILS in comparison to the reference TaBN absorber. Comparing Figure 8 (b) with Figure 7 (b) the TaCo alloy presents a reduction in best focus variation through pitch. This phenomenon is also attributed to the higher k value of the TaCo alloy. These observations are in accordance with what Philipsen et al. [21] have anticipated for high k materials. From an illumination source standpoint, the TCE graph for the TaCo alloy shows a similar pattern as the reference TaBN absorber. The TaCo alloy exhibits an increased TCE in comparison to TaBN for the respective illumination sources. As observed in Section 3.3, NILS and TCE exhibit trade-off, and NILS has been prioritized during the optimization process. Comparing Figure 8 (d) to Figure 7 (d) shows that Ta-Co alloys have a lower threshold-to-size value than the TaBN absorber which is as expected. High k materials result in lower EUV reflectivity and, as a result, a reduction in TtS is observed. Similar to TaBN, the illumination source does not seem to have much impact on the TtS values for horizontal LnS pattern using TaCo alloy. These findings only apply to the imaging metrics values evaluated with the bias shown in Figure 8 (f).

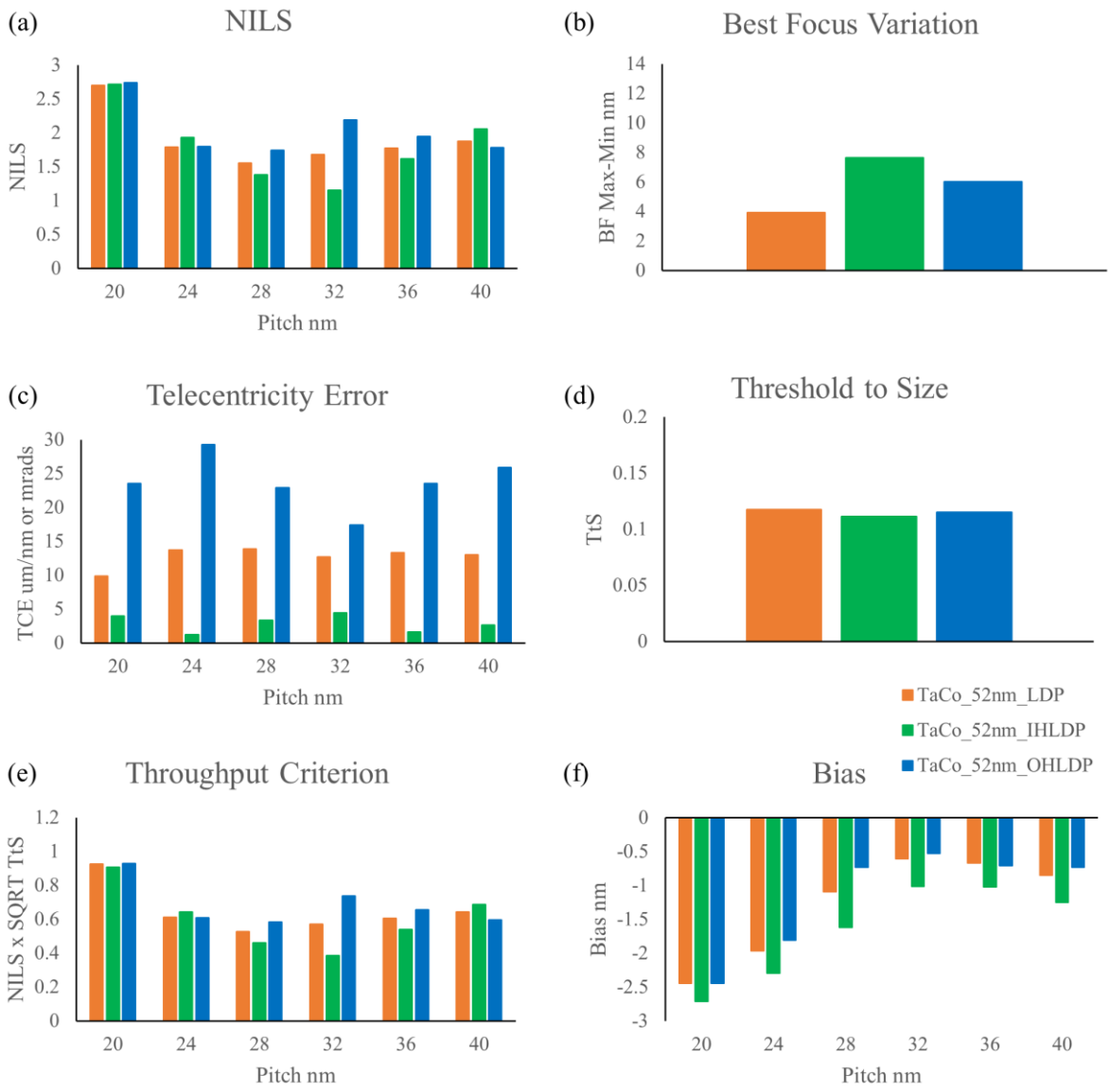

Figure 8. Comparison of the through-pitch imaging performance of TaCo alloy absorber for horizontal LnS pattern using different illumination source shapes (a) NILS, (b) best focus variation through pitch, (c) telecentricity error, (d) threshold-to-size, (e) throughput criterion, (f) mask bias.

A similar through-pitch comparison of different imaging metrics is made with vertical LnS pattern using different illumination source shapes for the reference TaBN absorber (Figure 9) and TaCo alloy (Figure 10). Almost identical observations can be found for all the imaging metrics under consideration.

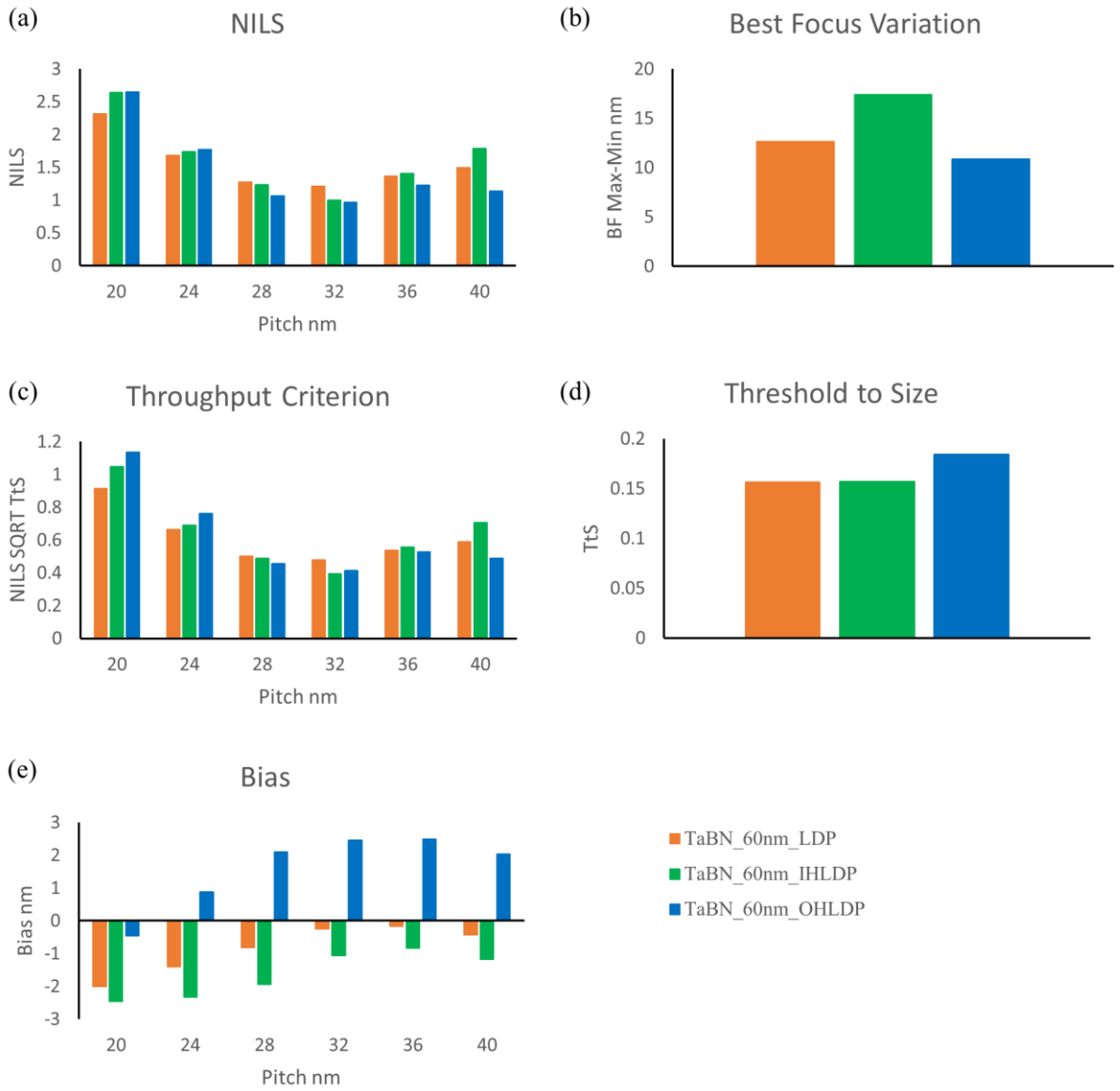

Figure 9. Comparison of the through-pitch imaging performance of reference TaBN absorber for vertical LnS pattern using different illumination source shapes (a) NILS, (b) best focus variation through pitch, (c) throughput criterion, (d) threshold-to-size, (e) mask bias

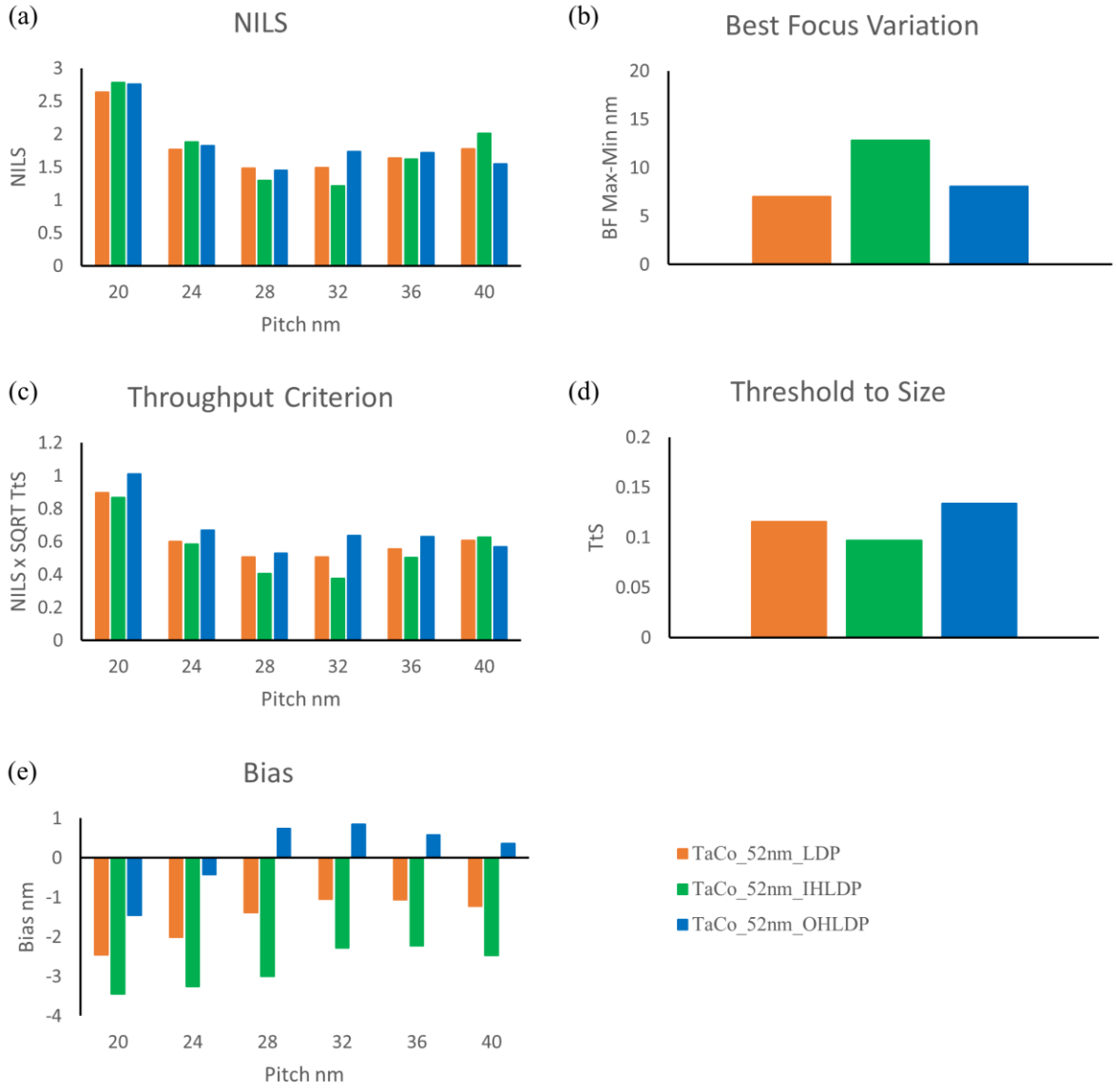

Figure 10. Comparison of the through-pitch imaging performance of TaCo alloy absorber for vertical LnS pattern using different illumination source shapes (a) NILS, (b) best focus variation through pitch, (c) throughput criterion, (d) threshold-to-size, (e) mask bias

4. Summary & Conclusion

Based on the state-of-the-art knowledge, we have proposed a methodology to facilitate absorber thickness optimization. By employing a case study of TaCo alloy, we were able to show how this technique may be used to a novel absorber while simultaneously validating it for the reference TaBN absorber. We observed the trends in the NILS plot as a function of absorber thickness and have made efforts to justify them by studying the diffraction orders. We conclude that multiple objectives such as TpT criterion, amplitude ratio and phase difference between diffraction orders require careful consideration to deduce the optimum absorber thickness.

We also observed the impact of illumination source shapes and trade-offs on the imaging metrics. The optical properties of an absorber in combination with illumination source shape produce case specific results for the imaging performance. The best illumination source shape for one type of absorber might not be the best choice for another type of absorber. Therefore, it is beneficial to use a TS-PS illumination for the thickness optimization with an emphasis on NILS as a primary criterion for lower defectivity and lower dose sensitivity. Additionally, the benefit of using a TS-PS illumination is that fewer computations are required. NILS plot obtained using TS-PS follows the same swing pattern through thickness as the other illumination sources under investigation. Therefore, a TS-PS can be used as a true representative of the illumination source shapes to investigate NILS behavior for the purpose of optimizing absorber thickness. Once the absorber thickness is fixed, a through-pitch evaluation using a full-fledged illumination source is suggested. To meet the specifications of lithography imaging performance, SMO (Source Mask Optimization) approaches may be helpful. The study also confirms that TaCo alloy exhibits improved NILS and lower BFV compared to the reference TaBN 60 nm absorber because of its high extinction coefficient *k*.

Acknowledgements

Authors would kindly like to thank Joern-Holger Franke (IMEC), Peter De Bisschop (IMEC), Lieve van Look (IMEC), Vincent Wiaux (IMEC) and Eelco van Setten (ASML) for the technical discussions.

REFERENCES

[1] Martin Burkhardt, Zheng Chen, Scott Halle, Romain Lallement, Stuart Sieg, Luciana Meli, "Focus considerations of design pitches and absorber choice for EUV random logic," Proc. SPIE 12051, Optical and EUV Nanolithography XXXV, 120510C (26 May 2022); https://doi.org/10.1117/12.2614296

[2] Andreas Erdmann, Peter Evanschitzky, Gerardo Bottiglieri, Eelco van Setten, Timon Fliervoet, "3D mask effects in high NA EUV imaging," Proc. SPIE 10957, Extreme Ultraviolet (EUV) Lithography X, 109570Z (26 March 2019); https://doi.org/10.1117/12.2515678

[3] Martin Burkhardt, "Investigation of alternate mask absorbers in EUV lithography," Proc. SPIE 10143, Extreme Ultraviolet (EUV) Lithography VIII, 1014312 (27 March 2017); https://doi.org/10.1117/12.2258266

[4] M.-Claire van Lare, Frank J. Timmermans, Jo Finders, "Alternative reticles for low-k1 EUV imaging," Proc. SPIE 11147, International Conference on Extreme Ultraviolet Lithography 2019, 111470D (26 September 2019); https://doi.org/10.1117/12.2536415

[5] Andreas Erdmann, Peter Evanschitzky, Hazem Mesilhy, Vicky Philipsen, Eric Hendrickx, Markus Bauer, "Attenuated PSM for EUV: Can they mitigate 3D mask effects?," Proc. SPIE 10583, Extreme Ultraviolet (EUV) Lithography IX, 1058312 (19 March 2018); https://doi.org/10.1117/12.2299648

[6] Devesh Thakare, Meiyi Wu, Karl Opsomer, Christophe Detavernier, Philipp Naujok, Qais Saadeh, Victor Soltwisch, Annelies Delabie, Vicky Philipsen, "Evaluation of Ta-Co alloys as novel high-k EUV mask absorber," Proc. SPIE 12051, Optical and EUV Nanolithography XXXV, 120510D (26 May 2022); https://doi.org/10.1117/12.2614235

[7] Eelco van Setten, Gerardo Bottiglieri, Laurens de Winter, John McNamara, Paul Rusu, Jan Lubkoll, Gijsbert Rispens, Jan van Schoot, Jens Timo Neumann, Matthias Roesch, Bernhard Kneer, "Edge placement error control and Mask3D effects in High-NA anamorphic EUV lithography," Proc. SPIE 10450, International Conference on Extreme Ultraviolet Lithography 2017, 104500W (30 October 2017); https://doi.org/10.1117/12.2280624

[8] I. A. Makhotkin, M. Wu, V. Soltwisch, F. Scholze, and V. Philipsen, "Refined extreme ultraviolet mask stack model," J. Opt. Soc. Am. A 38, 498-503 (2021)
[9] Claire van Lare, Frank Timmermans, Jo Finders, "Mask-absorber optimization: the next phase," J. Micro/Nanolith. MEMS MOEMS 19(2) 024401 (6 May 2020) https://doi.org/10.1117/1.JMM.19.2.024401
[10] Andreas Erdmann, Peter Evanschitzky, Gerardo Bottiglieri, Eelco van Setten, Timon Fliervoet, "3D mask effects in high NA EUV imaging," Proc. SPIE 10957, Extreme Ultraviolet (EUV) Lithography X, 109570Z (26 March 2019); https://doi.org/10.1117/12.2515678
[11] Andreas Erdmann, Peter Evanschitzky, Giuseppe Citarella, Tim Fühner, Peter De Bisschop, "Rigorous mask modeling using waveguide and FDTD methods: an assessment for typical hyper-NA imaging problems," Proc. SPIE 6283, Photomask and Next-Generation Lithography Mask Technology XIII, 628319 (19 May 2006); https://doi.org/10.1117/12.681872
[12] Joern-Holger Franke, Joost Bekaert, Victor Blanco, Lieve Van Look, Felix Wahlisch, Kateryna Lyakhova, Paul van Adrichem, Mark John Maslow, Guido Schiffelers, Eric Hendrickx, "Improving exposure latitudes and aligning best focus through pitch by curing M3D phase effects with controlled aberrations," Proc. SPIE 11147, International Conference on Extreme Ultraviolet Lithography 2019, 111470E (26 September 2019); https://doi.org/10.1117/12.2537104
[13] Natalia Davydova, Jo Finders, John McNamara, Eelco van Setten, Claire van Lare, Joern-Holger Franke, Andreas Frommhold, Renzo Capelli, Grizelda Kersteen, Andreas Verch, Rene Carpaij, Joseph Zekry, Timon Fliervoet, "Fundamental understanding and experimental verification of bright versus dark field imaging," Proc. SPIE 11517, Extreme Ultraviolet Lithography 2020, 115170P (30 October 2020); https://doi.org/10.1117/12.2573161
[14] Chen, Yulu & Sun, Lei & Qi, Zhengqing & Zhao, Shuo & Goodwin, Francis & Matthew, Itty & Plachecki, Vince. (2017). Tip-to-tip variation mitigation in extreme ultraviolet lithography for 7 nm and beyond metallization layers and design rule analysis. Journal of Vacuum Science & Technology B, Nanotechnology and Microelectronics: Materials, Processing, Measurement, and Phenomena. 35. 06G601. 10.1116/1.4994908
[15] Bartosz Bilski, Jörg Zimmermann, Matthias Roesch, Jack Liddle, Eelco van Setten, Gerardo Bottiglieri, Jan van Schoot, "High-NA EUV imaging: challenges, status and outlook," [Conference Presentation] Photo Mask Japan April 2021
[16] Eelco van Setten, Gerardo Bottiglieri, Laurens de Winter, John McNamara, Paul Rusu, Jan Lubkoll, Gijsbert Rispens, Jan van Schoot, Jens Timo Neumann, Matthias Roesch, Bernhard Kneer, "Edge placement error control and Mask3D effects in High-NA anamorphic EUV lithography," Proc. SPIE 10450, International Conference on Extreme Ultraviolet Lithography 2017, 104500W (30 October 2017); https://doi.org/10.1117/12.2280624
[17] C. Zahlten, P. Gräupner, J. van Schoot, P. Kürz, J. Stoeldraijer, W. Kaiser, "High-NA EUV lithography: pushing the limits," Proc. SPIE 11177, 35th European Mask and Lithography Conference (EMLC 2019), 111770B (29 August 2019)
[18] Jan Van Schoot, Eelco van Setten, Kars Troost, Sjoerd Lok, Judon Stoeldraijer, Rudy Peeters, Jos Benschop, Joerg Zimmerman, Paul Graeupner, Lars Wischmeier, Peter Kuerz, Winfried Kaiser, "High-NA EUV lithography exposure tool: program progress," Proc. SPIE 11323, Extreme Ultraviolet (EUV) Lithography XI, 1132307 (23 March 2020); https://doi.org/10.1117/12.2551491
[19] Erdmann, Andreas, Xu, Dongbo, Evanschitzky, Peter, Philipsen, Vicky, Luong, Vu and Hendrickx, Eric. "Characterization and mitigation of 3D mask effects in extreme ultraviolet lithography" Advanced Optical Technologies, vol. 6, no. 3-4, 2017, pp. 187-201. https://doi.org/10.1515/aot-2017-0019
[20] Andreas Erdmann, Hazem S. Mesilhy, Peter Evanschitzky, Vicky Philipsen, Frank J. Timmermans, Markus Bauer, "Perspectives and tradeoffs of absorber materials for high NA EUV lithography," J. Micro/Nanolith. MEMS MOEMS 19(4) 041001 (1 October 2020) https://doi.org/10.1117/1.JMM.19.4.041001
[21] Vicky Philipsen, Kim Vu Luong, Karl Opsomer, Christophe Detavernier, Eric Hendrickx, Andreas Erdmann, Peter Evanschitzky, Robbert W. E. van de Kruijs, Zahra Heidarnia-Fathabad, Frank Scholze, Christian Laubis, "Novel EUV mask absorber evaluation in support of next-generation EUV imaging," Proc. SPIE 10810, Photomask Technology 2018, 108100C (10 October 2018); https://doi.org/10.1117/12.2501799

[22] Jan Van Schoot, Sjoerd Lok, Eelco van Setten, Ruben Maas, Kars Troost, Rudy Peeters, Jo Finders, Judon Stoeldraijer, Jos Benschop, Paul Graeupner, Peter Kuerz, Winfried Kaiser, "High-NA EUV lithography exposure tool: advantages and program progress," Proc. SPIE 11517, Extreme Ultraviolet Lithography 2020, 1151712 (7 January 2021); https://doi.org/10.1117/12.2572932

[23] Joern-Holger Franke, Joost Bekaert, Victor Blanco, Lieve Van Look, Felix Wahlisch, Kateryna Lyakhova, Paul van Adrichem, Mark John Maslow, Guido Schiffelers, Eric Hendrickx, "Improving exposure latitudes and aligning best focus through pitch by curing M3D phase effects with controlled aberrations," Proc. SPIE 11147, International Conference on Extreme Ultraviolet Lithography 2019, 111470E (26 September 2019); https://doi.org/10.1117/12.2537104

[24] Martin Burkhardt, "Investigation of alternate mask absorbers in EUV lithography," Proc. SPIE 10143, Extreme Ultraviolet (EUV) Lithography VIII, 1014312 (27 March 2017); https://doi.org/10.1117/12.2258266